

Alternating Bias Assisted Annealing of Amorphous Oxide Tunnel Junctions

D. P. Pappas,^{1,*} M. Field,¹ C. Kopas,¹ J. A. Howard,¹ X. Wang,¹ E. Lachman,¹ Lin Zhou,^{2,3} Jinsu Oh,^{2,3} K. Yadavalli,¹ E. A. Sete,¹ A. Bestwick,¹ M.J. Kramer,^{2,3} and J. Y. Mutus¹

¹*Rigetti Computing, 775 Heinz Avenue, Berkeley, CA 94710, USA*

²*Ames National Laboratory, Ames, IA 50011, USA*

³*Department of Materials Science and Engineering, Iowa State University, Ames, IA 50011, USA*

(Dated: February 28, 2024)

We demonstrate a transformational technique for controllably tuning the electrical properties of individual aluminum-oxide tunnel junctions. Using conventional test equipment to apply an alternating bias to a heated tunnel barrier, giant increases in the room temperature resistance, greater than 70%, can be achieved. The rate of resistance change is shown to be strongly temperature-dependent, and is weakly dependent on junction size in the sub-micron regime. In order to measure their tunneling properties at mK temperatures, we characterized transmon qubit junctions treated with this alternating-bias assisted annealing (ABAA) technique. The measured frequencies follow the Ambegaokar-Baratoff relation between the shifted resistance and critical current. Further, these studies show a reduction of junction-contributed loss on the order of $\approx 0.3 \times 10^{-6}$, and indicate that there is a reduction in resonant-and off-resonant-two level system defects when compared to untreated samples. Imaging with high-resolution TEM shows that the barrier is still predominantly amorphous with a more uniform distribution of aluminum coordination across the barrier relative to untreated junctions. This new approach is expected to be widely applicable to a broad range of devices that rely on amorphous aluminum oxide, and is likely applicable to many other metal-insulator-metal devices.

I. INTRODUCTION

The preparation of amorphous thin film materials is surprisingly simple. While devices incorporating these materials are ubiquitous, their morphology is surprisingly complex and challenging to control. Among other similar materials, amorphous aluminum oxide tunnel (a- AlO_x) junctions stand out due to their importance in both cryogenic and room temperature devices. These applications range from those that utilize the Josephson effect [1], such as SQUID magnetometers [2], superconducting qubits [3, 4], amplifiers [5, 6], RSFQ logic [7], to room temperature magnetic tunnel junctions [8] and memory elements [9–11].

Due to the cryogenic application of these oxide barriers for Josephson junctions, we can probe not only their resistance but also the prevalence of defects and loss using superconducting qubits. This is especially relevant to the field of quantum information since a- AlO_x is a key ingredient in transmon qubits [15], the invention of which has fueled much of the rapid development of superconducting applications research over the past decade. The junction properties are crucial in the overall properties and performance of the qubit. Most importantly, the critical current, I_c of the barrier sets the Josephson energy of the device, $E_J = I_c \Phi_0 / 2\pi$, where Φ_0 is the flux quantum, which determines the parameters such as the frequency, anharmonicity, and charge noise sensitivity. Specifically, I_c can be predicted by the Ambegaokar-Baratoff formula, i.e. $I_c = \pi \Delta / 2eR_n$ [16], where, the variables R_n and Δ

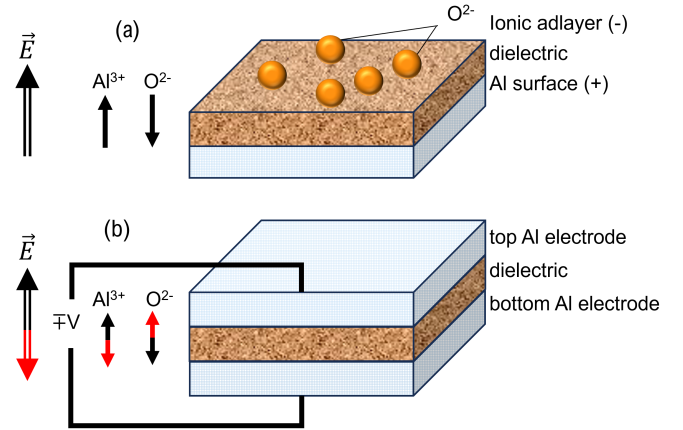


FIG. 1. (a) Oxide growth on aluminum according to the Cabrera-Mott mechanism [12, 13]. The primary assumption is that electrons freely ionize adsorbed oxygen. This creates a voltage V_{Mott} relative to the Al, causing a strong electric field in the thin oxide. Due to the predominantly ionic-bonded nature of these films (56%) [14], aluminum cations and oxygen anions feel opposite forces due to this field. They exchange places, mediated by vacancy motion. (b) Method of mixing the Al/ AlO_x /Al trilayer by applying alternating voltages, on the order of magnitude of V_{Mott} but less than the dielectric breakdown voltage [11], between the two plates. This applies alternating and opposing forces on the two species.

are the resistance of the junction (in its normal state) and the superconducting gap of the electrodes.

Unfortunately, while it is essential that I_c , and hence R_n , is well defined, a large spread of R_n in nominally identical junctions is typically observed, on the order of 1-10% at the wafer level [17]. This is due to both intrinsic

* dpappas@rigetti.com

sic properties and extrinsic effects. Intrinsic issues include the exponential dependence of the tunneling on the thickness [18]; grain structure; and interface roughness. Extrinsic effects arise from the effects of lithography uncertainties [19], processing, electrostatic sensitivity, and circuit design.

Moreover, the amorphous nature of the oxide layer results in the inclusion of defects that can cause two-level systems (TLS's) near the qubit frequency that typically reduce coherence, or the defects can result in two-level fluctuators (TLF's) at very low frequencies that push the qubit frequency around [20, 21].

The default method of making junctions, also used in this work, employs thermal oxidation of an aluminum surface described by the Cabrera-Mott model which shows the initial oxidation is driven by an intrinsic electric field [12, 13]. This process is convenient and powerful because it is conformal and self-limiting in thickness. In the thin-barrier limit the formation of the oxide barrier is governed by drift-dominated atomic diffusion [13, 22] of the charged constituent elements, Al^{3+} and O^{2-} , in opposite directions, as illustrated in Fig. 1 (a). This diffusion is driven by the strong E -field ~ 1 GV/m generated by the adsorbed ionic ad-layer. In these, and other metal-insulator-metal oxides, the relevant parameter is referred to as the Mott voltage, $V_{\text{Mott}} \approx 0.5\text{-}1$ V for aluminum oxide [23].

There have been many efforts to improve the properties of the a- AlO_x material, focused primarily on understanding and optimizing the junction formation and post-processing, i.e. pressure, time, [24], interface preparation, etches, simulations, etc., see Ref. [25, 26] and citations therein. These efforts have met with limited success, and it is typically assumed that the properties of the junctions, as formed, are relatively frozen-in and difficult to adjust. For example, annealing the junctions to high temperatures can significantly change significant the resistance[?], globally heating many junctions has limited efficacy due to nano-scopic morphology differences of nominally identical junctions at the domain and atomic level. Since the resistance tends to increase on continued annealing, novel approaches to sequentially targeting the junctions have been useful in mitigating these spreads by targeting a slightly lower resistance than desired and then locally heating the individual junctions to bring them into tolerance [27–30]. However, these procedures involve the addition of optical elements to the test and measurement apparatus and appear to be limited to adjustments of the resistances up to about 10-12% in Al/a- AlO_x /Al junctions, i.e. on the order of the junction spread. This limits the number of junction arrays that can be successfully adjusted, based on the initial distribution of the junctions.

On the other hand, it has been shown that oxidation can be enhanced by an external voltage [31], for example, that generated by e-beam bombardment at the surface [32]. When comparing with other physical material systems, e.g. magnetic [33] and piezo-electric [34], where

annealing while applying an alternating field polarity can have significant positive effects [8, 35], this approach has not yet been investigated in connection to a- AlO_x only tunnel junctions and is illustrated in Fig 1(b).

II. EXPERIMENTAL SETUP AND RESULTS ON JUNCTIONS

In this work, we have investigated this approach in a protocol that we refer to as alternating bias-assisted anneal (ABAA). The ABAA technique entails applying an alternating polarity voltage pulse train to the junctions during a global, low-temperature anneal. ABAA can be implemented using a conventional probe station with a low-temperature heating stage, as illustrated in Fig. 2. Using this technique, it can be expected that the Al^{3+} cations and O^{2-} anions in the barrier will be driven in opposite directions at each pulse. By alternating the bias voltage the ions can be driven out of local, metastable sites into a lower energy configuration. In general, the guidelines used for the voltage profiles were that it should be on the order of V_{Mott} and less than the breakdown voltage, $V_B \sim 1.5$ V [11, 23]. When considering the time duration of the pulse, we note that by staying well below V_B the junction properties were observed to evolve relatively slowly, on the order of 100's of seconds, similar to the known oxidation rates of these surfaces. Finally, a relatively low temperature is desired to not expose junctions to a higher temperature than the highest temperature they are exposed to during the fabrication process.

The equipment and pulse sequences used for the tuning consist of a standard source-measure unit (SMU) and a probe station with a heated platen, illustrated in Fig. 2(a,b). The SMU was programmed to provide a train of 1-second-long anneal-assist pulses after the wafer was brought to the target temperature. The pulse amplitudes were set in the range of 0.8 - 1.1 V. The resistance of the junctions was measured after each pulse with an additional pulse at low voltage. As shown in Fig. 2(d), when unipolar pulse trains were applied to the junctions a relatively small change in the resistance was observed. Changes of about 2% and 6%, respectively, were registered for negative-only and positive-only voltages after about 200 pulses. However, when alternating-polarity-bias (AB) pulses were used, as illustrated in Fig. 2(c), resistance changes of more than 70% were recorded as shown in Fig. 2(d). In addition, we note two new features of the ABAA process that we address later in this paper: first, that a cyclic response was typically observed for the AB pulse trains, as illustrated in the Fig. 2(d) inset; and second, a systematic jump in the resistance curve typically occurs during the process.

Further studies including the temperature dependence of this effect are shown in Fig. 3. We find the rate increases significantly as the temperature is increased from 25 up to 80°C. The increase is on the order of $2\times$ every

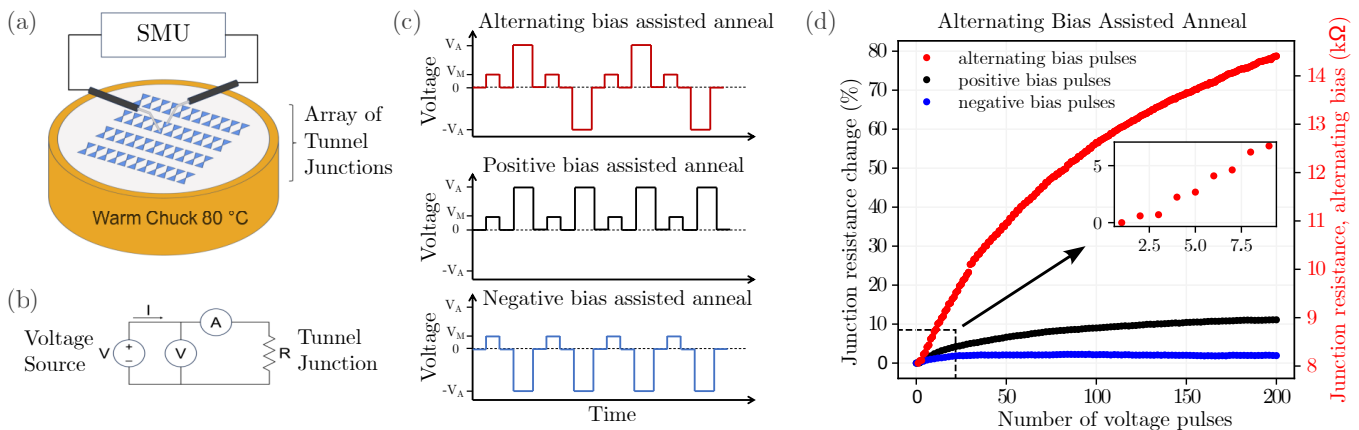


FIG. 2. Schematic diagram of the bias schemes used to anneal tunnel junctions. (a) A block diagram of the apparatus. In all cases, the voltage source has the positive terminal connected to the top electrode and the negative terminal connected to the bottom electrode sitting on the substrate. (b) A circuit diagram. (c) Bias pulses at V_A are applied for 1 second. In this paper $V_A = 0.9$ V. Between the bias pulses a low measurement pulse of $V_M = 10$ mV is used to measure the low bias resistance of the junction. (d) Data for voltage-assisted annealing using alternating bias assisted anneal (ABAA) at 80°C vs. unipolar (positive and negative w.r.t. the top electrode) voltage pulses. The maximum voltage amplitude $V_A = \pm 0.9\text{V}$ with a 1-second pulse length. The area of the junction under test is $1.55 \mu\text{m} \times 0.24 \mu\text{m} = 0.37 (\mu\text{m})^2$. The inset is a zoom in on the start of the ABAA process and shows the cyclic change in junction resistance with a repeated sequence of small and large resistance changes when applying alternating bias bipolar pulses.

10°C , consistent with that expected from an Arrhenius law. On the other hand, the size dependence (shown in the supplement) is flat over more than an order of magnitude, indicating that the mechanism is not due to the

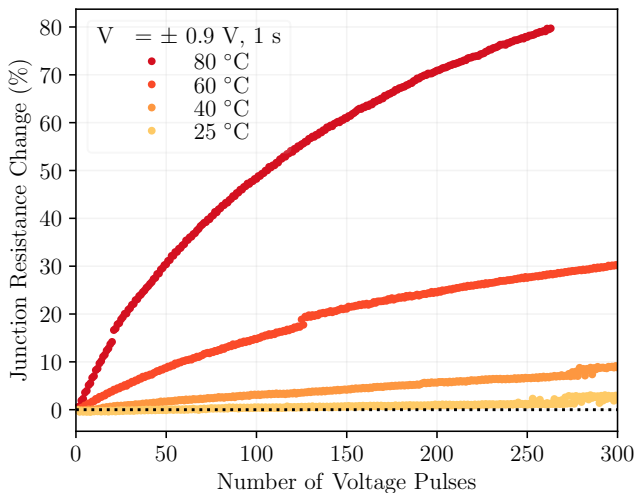


FIG. 3. Junction resistance change as a function of the number of AB pulses for four nominally identical junctions from the same wafer at different substrate temperatures. In addition to the relatively smooth increase in junction resistance as the AB pulses are applied, discontinuities can often be observed as single events as in the process conducted at higher temperatures. In general, the annealing voltage amplitudes (for either polarity), pulse duration, and temperature are related. Further explorations of these parameters are ongoing.

perimeter or other side effects. This points to local effects such as reordering and increased coordination of the atoms in the barrier, leading to changes in the effective barrier height as atoms reach a more stable configuration or interfacial modifications such as smoothing or thickening of the barrier. Furthermore, since the data was taken at constant voltage, we infer that it is not a current-driven diffusion effect. This has more practical implications from the perspective of SQUID-based devices, such as sensors and tunable qubits, because these devices are typically made using two parallel circuits with junctions that may or may not be the same size. Finally, we note that the resistance jumps are also evident in the 25, 40, and 60°C data.

III. EFFECT OF ABAA ON TRANSMON QUBITS

We probe the effect of ABAA on the tunneling properties of the barrier by characterizing transmon qubits taken with and without ABAA. We measure a variety of properties associated with the junctions: whether I_C follows the behavior expected by the Ambegaokar-Baratoff relationship, the impact of the barrier on qubit loss, and the presence of strongly coupled TLS's. We measured both tunable and fixed-frequency qubits [36]. For the coherence and TLS tests, we selected 5 equivalent chips from the same wafer, each containing nominally 16 qubits; 14 flux-tunable and two fixed qubits. Two chips were control devices with no ABAA process (unprocessed). Of the three remaining chips, all were processed to 80°C , but qubits on one and a half chips only (24 in

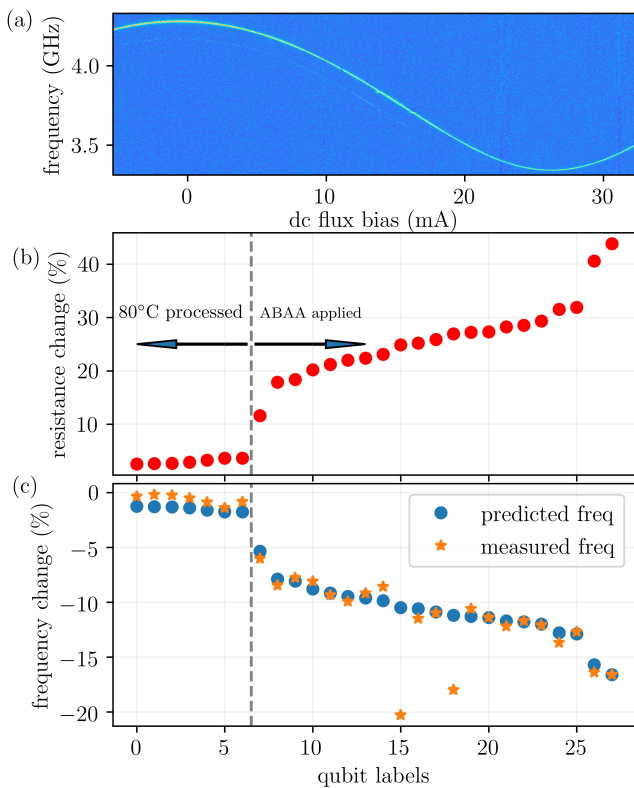


FIG. 4. Summary of qubit characterizations. (a) A spectrum of a tunable qubit that has been treated with ABAA. Two small features in Fig 4(a) at $\tilde{3}.8$ GHz and $\tilde{3}.7$ GHz correspond to neighboring qubits. (b) Measured junction resistance shift (red dots) resulting from the ABAA trimming of junctions. (c) The blue dots show the predicted frequency change from untreated values using the Ambegaokar-Baratoff relation while the orange stars show the measured frequency change. Critical currents from about 20-30 nA for the treated junctions were estimated (see supplement).

total) were processed with ABAA. Among the 24 ABAA processed qubits, 3 failed to a short circuit and 6 others lost tunability (we plan to understand failure mode as part of future work). Among qubits in the control group or those that were processed through 80C but not ABAA, we had a couple failed qubits each at cryogenic temperatures which showed expected room-temperature resistance measurements, possibly due to handling related issues.

The Ambegaokar-Baratoff parameter set for this ensemble was first determined using the untreated devices. Then the measured frequencies of the treated qubits were calculated for various resistance-trimming amounts. For the non-tunable qubits, this is straightforward, while for the tunable qubits, it is necessary to find the maximum frequency, i.e., zero flux-bias point. This process is illustrated in Fig 4(a), showing the spectrum of a tunable qubit. It can also be seen in Fig 4(b) that the predicted and measured frequencies for ABAA treated qubits match well, as discussed more in depth later.

The qubit spectroscopy also probes for the existence of avoided level crossings in this frequency range. Such crossings are signatures of strongly coupled TLS defects within the tunnel barrier. [37, 38] For reference, measurements on unprocessed qubits show about 0.7 TLS/GHz, and on those that were heated to 80°C have 0.6 TLS/GHz.

Compared to these measurements, for this qubit and all of the other tunable devices in the ABAA-treated ensemble we found no evidence of avoided level crossings. Over the total frequency range of 5.4 GHz in 9 tunable qubits, we would have expected at least a few avoided-level TLS signatures based on the above reference data. Furthermore, the low-frequency stability of one of the devices was monitored over many hours and there was no evidence of coupling to TLFs [21], as illustrated in the supplement. We note here that smaller splittings, typically detected with swap spectroscopy [38] and likely due to surface defects, would not be affected by the ABAA. While this small data set is not conclusive evidence that such defects are suppressed by the ABAA process, it does point to the possibility that ABAA may improve qubit coherence and frequency stability. In order to investigate this possibility further, we studied the loss and time domain coherence in the ABAA qubit ensemble.

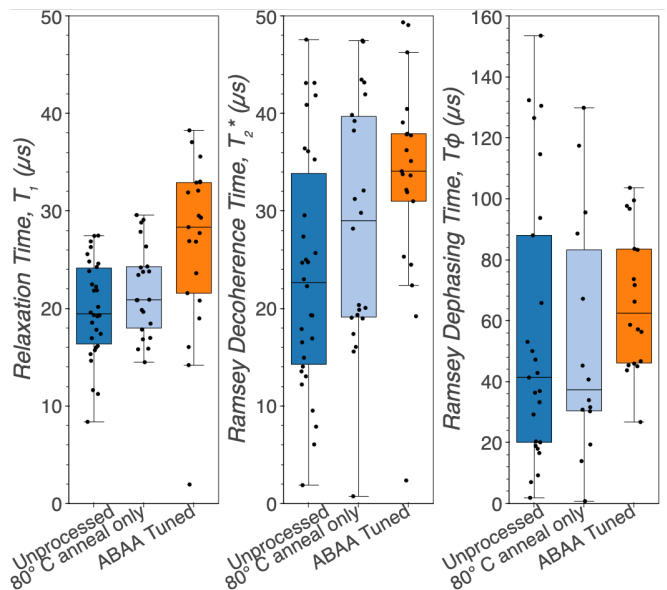


FIG. 5. Summary of qubit lifetimes. (a): Qubit relaxation time, (b): Qubit Ramsey decoherence time, and (c) Qubit dephasing time for three populations of qubits: unprocessed, annealed to 80 °C, and tuned using ABAA with $V_A = 1$ V, 1 s and $T = 80^\circ\text{C}$. The number of measured qubits in the Unprocessed data set is $n_{\text{qubit}} = 30$, the 80°C anneal only has $n_{\text{qubit}} = 22$, and the ABAA tuned set has $n_{\text{qubit}} = 21$.

In Figure 5 and tabulated in the supplement, we show coherence metrics for all qubits measured in the study. Here, each data point corresponds to the median of at least 60 measurements on one particular qubit. We observe that the ABAA processed devices have a higher

median T_1 than both the unprocessed and the devices that were only heated to 80°C, although the T_2^* and T_ϕ values between sample sets are not distinguishable within the spread of the values.

When analyzing processes that may reduce loss in qubits, it is useful to compare these metrics in the form of a qubit decay rate normalized to frequency ($1/(T_1 \times (2\pi f_{01}))$); the ABAA tuned sample set has median loss tangent of 1.4×10^{-6} , while both the 80°C annealed and unprocessed sets have median loss tangents of 1.7×10^{-6} . We found that the coherence was typically improved after the ABAA process, indicating that the resistance trimming may have reduced the median loss tangent in the junction by about 0.3×10^{-6} . Furthermore, the effects of the resistance trimming on the qubit frequencies are shown in Fig. 4(b), where we see that the increase of the resistance results in a reduced measured frequency, shown in Fig. 4(c) as orange stars. The expected frequencies (blue circles), compare well with the measured values. We also find the Ambegaokar-Baratoff relationship is consistent between junctions with ABAA applied vs. unprocessed with values of (1.32 ± 0.084) pH/ Ω and (1.27 ± 0.109) pH/ Ω respectively.

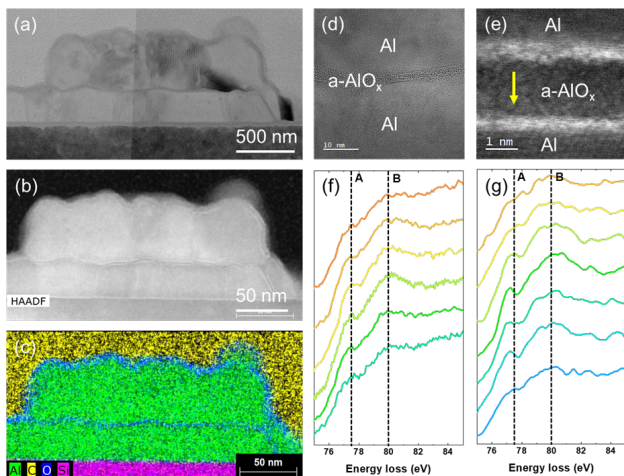


FIG. 6. Electron microscopy analysis on ABAA-treated junction. (a) a low-magnification cross-sectional TEM image of the junction. (b) a HAADF-STEM image and (c) a corresponding STEM-EDS elemental distribution map. (d) High-resolution TEM image of Al/a-AlO_x/Al interfaces. (e) HAADF-STEM image of Al/a-AlO_x/Al interfaces. (f) ELNES of Al₂₃ edge of the ABAA-treated sample taken from the yellow arrow indicated region in (e), and (g) ELNES of Al₂₃ edge of the untreated a-AlO_x barrier from reference [39]

Finally, TEM imaging and EELS analysis were employed to investigate morphological changes in the junctions due to the ABAA process. These studies indicate that the increase in junction resistivity may be attributed to a more uniform barrier structure with reduced point defect density. A low-mag cross-sectional TEM/STEM image and corresponding EDS elemental

distribution map are shown in Fig. 6(a-c) showing that a-AlO_x barrier is still amorphous in the ABAA-treated sample (Fig. 6(d)), and the HAADF-STEM image shows a barrier thickness of approximately 2 nm (Fig. 6(e)).

While the ABAA technique does not appear to change the amorphous nature of the barrier from visual inspection, the chemical analysis tells a different story. We see a much more homogeneous chemistry in the ABAA-treated a-AlO_x than in untreated junctions. Our previous research showed that the distance between two main peaks labeled as A and B in Fig. 6(f-g), close to approximately 77.5 eV and 80 eV of the Al L₂₃ energy-loss near edge structure (ELNES) respectively, can be used to analyze the coordination number of Al [39–44]. Specifically, the Al L₃ edges (peak A) tends to shift to higher energy as Al coordination numbers increase. For untreated junctions, a spatial variation in coordination number across the a-AlO_x barrier from the untreated junction (Fig. 6(g)) [39] is demonstrated and considered as a potential decoherence source. In contrast, the ABAA-treated junction shows a uniform distribution of Al coordination number through the barrier, as the peak positions of A and B remain unchanged across the a-AlO_x layer, as shown in Fig. 6(f). This may originate from the migration/recombination of charged point defects induced by the alternating bias field [45] giving rise to a more chemically homogeneous barrier layer. This effect may increase the effective barrier height of the tunnel junction leading to the observed increase in resistance.

IV. CONCLUSION

We find that an alternating bias is effective in assisting the thermal annealing of a diatomic amorphous material, similar to adding restarts in simulated annealing solver to avoid local minima [46]. This allows for significant modifications of the junction resistance, in excess of +70%, with apparent reductions in loss and defects. The behavior of the resistance during the ABAA process showed cyclic small and large changes in resistance as the positive- and negative-bias voltages were applied and the junction resistance increased, and typically a single discontinuity in resistance was observed if sufficient number of pulses were applied. These results along with the temperature-dependent studies and imaging point to an assisted annealing mechanism, for example, improved local ordering and/or the a-AlO_x being driven into a lower-energy glassy state[47, 48] in the potential energy landscape, as is indicated by the observed reduction in loss and TLS. In order to confirm these hypotheses, more studies such as high-resolution imaging and molecular dynamics that include density-functional theory are required. Regardless of the mechanism, we expect that a controlled alternating bias-assisted junction annealing approach will pave the way for building large-scale superconducting quantum processors by improving qubit frequency targeting, coherence, and stability. Other ap-

lications where targeting tunnel junction resistance is important may benefit by allowing for more homogeneous junction chains and ensembles for devices ranging from amplifiers to voltage standards, sensors, and data storage.

ACKNOWLEDGMENTS

The structural and chemical characterization and analysis is based upon work supported by the U.S. Department of Energy, Office of Science, National Quantum

Information Science Research Centers, Superconducting Quantum Materials and Systems Center (SQMS) under contract number DE-AC02-07CH11359. We acknowledge the support of Anna Grassellino and Akshay Murthy. All resistance measurements were conducted on FormFactor automated probe stations with the help of Anwar Aslam, Connor Smith, and Brandon Boiko. We thank Hilal Cansizoglu and the Rigetti fab team members for junction process development and samples, as well as Rory Cochrane and Cassidy Berk for assistance with cryogenic measurements and TLS analysis. We thank Greg Stiehler for his critical eye in preparation of this manuscript.

-
- [1] B.D. Josephson, "Possible new effects in superconductive tunnelling," *Physics Letters* **1**, 251–253 (1962).
- [2] J. Clarke, *The SQUID handbook Vol 1 Fundamentals and technology of SQUIDS and SQUID systems* (Wiley VCH, Germany, 2004).
- [3] M. H. Devoret, *Quantum fluctuations in electrical circuits* (Edition de Physique, France, 1997).
- [4] Y. Nakamura, Yu. A. Pashkin, and J. S. Tsai, "Coherent control of macroscopic quantum states in a single-cooper-pair box," *Nature* **398**, 786–788 (1999).
- [5] Manuel A. Castellanos-Beltran, Kent D. Irwin, Leila R. Vale, Gene C. Hilton, and Konrad W. Lehnert, "Bandwidth and dynamic range of a widely tunable josephson parametric amplifier," *IEEE Transactions on Applied Superconductivity* **19**, 944–947 (2009).
- [6] C. Macklin, K. O'Brien, D. Hover, M. E. Schwartz, V. Bolkhovskiy, X. Zhang, W. D. Oliver, and I. Siddiqi, "A near-quantum-limited josephson traveling-wave parametric amplifier," *Science* **350**, 307–310 (2015), <https://www.science.org/doi/pdf/10.1126/science.aaa8525>.
- [7] K.K. Likharev and V.K. Semenov, "Rsfq logic/memory family: a new josephson-junction technology for sub-terahertz-clock-frequency digital systems," *IEEE Transactions on Applied Superconductivity* **1**, 3–28 (1991).
- [8] Keerthana Shajil Nair, Marco Holzer, Catherine Dubourdieu, and Veeresh Deshpande, "Cycling Waveform Dependent Wake-Up and ON/OFF Ratio in Al₂O₃/Hf_{0.5}Zr_{0.5}O₂ Ferroelectric Tunnel Junction Devices," *ACS Applied Electronic Materials* **5**, 1478–1488 (2023).
- [9] Jian-Gang (Jimmy) Zhu and Chando Park, "Magnetic tunnel junctions," *Materials Today* **9**, 36–45 (2006).
- [10] W. H. Rippard, A. C. Perrella, F. J. Albert, and R. A. Buhrman, "Ultrathin aluminum oxide tunnel barriers," *Phys. Rev. Lett.* **88**, 046805 (2002).
- [11] J. J. O'Dwyer, "Current-Voltage Characteristics of Dielectric Films," *Journal of Applied Physics* **37**, 599–601 (2004), https://pubs.aip.org/aip/jap/article-pdf/37/2/599/7938519/599_1_online.pdf.
- [12] N Cabrera and N F Mott, "Theory of the oxidation of metals," *Reports on Progress in Physics* **12**, 163 (1949).
- [13] Xingfan Zhang, Peiru Zheng, Yingjie Ma, Yanyan Jiang, and Hui Li, "Atomic-scale understanding of oxidation mechanisms of materials by computational approaches: A review," *Materials & Design* **217**, 110605 (2022).
- [14] Linus Pauling, "The nature of the chemical bond. application of results obtained from the quantum mechanics and from a theory of paramagnetic susceptibility to the structure of molecules," *Journal of the American Chemical Society* **53**, 1367–1400 (1931).
- [15] J. Koch, M.Y. Terri, J. Gambetta, A.A. Houck, D.I. Schuster, J. Majer, A. Blais, M.H. Devoret, S.M. Girvin, and R.J. Schoelkopf, "Charge-insensitive qubit design derived from the cooper pair box," *Phys. Rev. A* **76**, 042319 (2007).
- [16] Charles van Duzer, Theodore; Turner, *Principles of Superconductive Devices and Circuits, 2nd ed.* (Prentice-Hall, Upper Saddle River NJ, 1999).
- [17] Nandini Muthusubramanian, Matvey Finkel, Pim Duivestein, Christos Zachariadis, Sean L. M. van der Meer, Hendrik M. Veen, Marc W. Beekman, Thijs Stavenga, Alessandro Bruno, and Leonardo DiCarlo, "Wafer-scale uniformity of dolan-bridge and bridgeless manhattan-style josephson junctions for superconducting quantum processors," *Quantum Science and Technology* (2023), 10.1088/2058-9565/ad199c.
- [18] Lunjie Zeng, Dung Trung Tran, Cheuk-Wai Tai, Gunnar Svensson, and Eva Olsson, "Atomic structure and oxygen deficiency of the ultrathin aluminium oxide barrier in Al/AlO_x/Al Josephson junctions," *Scientific Reports* **6**, 29679 (2016).
- [19] Alexander Bilmes, Alexander K Händel, Serhii Voloshe-niuk, Alexey V Ustinov, and Jürgen Lisenfeld, "In-situ bandaged josephson junctions for superconducting quantum processors," *Superconductor Science and Technology* **34**, 125011 (2021).
- [20] J.M. Martinis, K.B. Cooper, R. McDermott, M. Steffen, M. Ansmann, K.D. Osborn, K. Cicak, S. Oh, D.P. Pappas, R.W. Simmonds, *et al.*, "Decoherence in josephson qubits from dielectric loss," *Phys. Rev. Lett.* **95**, 210503 (2005).
- [21] Steffen Schlör, Jürgen Lisenfeld, Clemens Müller, Alexander Bilmes, Andre Schneider, David P. Pappas, Alexey V. Ustinov, and Martin Weides, "Correlating decoherence in transmon qubits: Low frequency noise by single fluctuators," *Phys. Rev. Lett.* **123**, 190502 (2019).
- [22] Zhijie Xu, Kevin M. Rosso, and Stephen Bruemmer, "Metal oxidation kinetics and the transition from thin to thick films," *Phys. Chem. Chem. Phys.* **14**, 14534–14539 (2012).

- [23] Na Cai, Guangwen Zhou, Kathrin Müller, and David E. Starr, “Temperature and pressure dependent Mott potentials and their influence on self-limiting oxide film growth,” *Applied Physics Letters* **101**, 171605 (2012), <https://pubs.aip.org/aip/apl/article-pdf/doi/10.1063/1.4764552/14257769/171605.1.online.pdf>.
- [24] William H. Mallison, “Dependence of Critical Current Density on Oxygen Exposure in Nb-AlO_x-Nb Tunnel Junctions,” *IEEE Transactions on Applied Superconductivity* **5**, 26–30 (1995).
- [25] Chang-Eun Kim, Keith G. Ray, and Vincenzo Lordi, “A density-functional theory study of the Al/AlO_x/Al tunnel junction,” *Journal of Applied Physics* **128**, 155102 (2020), <https://pubs.aip.org/aip/jap/article-pdf/doi/10.1063/5.0020292/14113892/155102.1.online.pdf>.
- [26] M. J. Cyster, J. S. Smith, N. Vogt, G. Opletal, S. P. Russo, and J. H. Cole, “Simulating the fabrication of aluminium oxide tunnel junctions,” *npj Quantum Information* **7**, 12 (2021).
- [27] C. Granata, A. Vettoliere, L. Petti, M. Ripa, B. Ruggiero, P. Mormile, and M. Russo, “Localized laser trimming of critical current in niobium based josephson devices,” *Applied Physics Letters* **90** (2007), 10.1063/1.2746060.
- [28] Jared B. Hertzberg, Eric J. Zhang, Sami Rosenblatt, Easwar Magesan, John A. Smolin, Jeng-Bang Yau, Vivekananda P. Adiga, Martin Sandberg, Markus Brink, Jerry M. Chow, and Jason S. Orcutt, “Laser-annealing josephson junctions for yielding scaled-up superconducting quantum processors,” *npj Quantum Information* **7**, 129 (2021).
- [29] Eric J. Zhang, Srikanth Srinivasan, Neereja Sundaresan, Daniela F. Bogorin, Yves Martin, Jared B. Hertzberg, John Timmerwilke, Emily J. Pritchett, Jeng-Bang Yau, Cindy Wang, William Landers, Eric P. Lewandowski, Adinath Narasgond, Sami Rosenblatt, George A. Keefe, Isaac Lauer, Mary Beth Rothwell, Douglas T. McClure, Oliver E. Dial, Jason S. Orcutt, Markus Brink, and Jerry M. Chow, “High-performance superconducting quantum processors via laser annealing of transmon qubits,” *Science Advances* **8**, eabi6690 (2022), <https://www.science.org/doi/pdf/10.1126/sciadv.abi6690>.
- [30] Hyunseong Kim, Christian Jünger, Alexis Morvan, Edward S. Barnard, William P. Livingston, M. Virginia P. Altoé, Yosep Kim, Chengyu Song, Larry Chen, John Mark Kreikebaum, D. Frank Ogletree, David I. Santiago, and Irfan Siddiqi, “Effects of laser-annealing on fixed-frequency superconducting qubits,” *Applied Physics Letters* **121**, 142601 (2022), <https://pubs.aip.org/aip/apl/article-pdf/doi/10.1063/5.0102092/16484380/142601.1.online.pdf>.
- [31] M. K. Konkin and J. G. Adler, “Annealing effects in tunnel junctions (voltage annealing),” *Journal of Applied Physics* **51**, 5450–5454 (2008), <https://pubs.aip.org/aip/jap/article-pdf/51/10/5450/7969138/5450.1.online.pdf>.
- [32] H. D. Ebinger and J. T. Yates, “Electron-impact-induced oxidation of Al(111) in water vapor: Relation to the Cabrera-Mott mechanism,” *Phys. Rev. B* **57**, 1976–1984 (1998).
- [33] Yide Zhang, “Magnetic annealing of magnetic alloys in a dynamic magnetic field,” (2001), uS Patent 6,217,672 B1.
- [34] Noriko Yamamoto, Yamashita, and et. al, “Ultrasonic probe, piezoelectric transducer, method of manufacturing ultrasonic probe, and method of manufacturing piezoelectric transducer,” (2014), uS Patent 2014/0062261 A1.
- [35] Riccardo Fontanini, Justine Barbot, Mattia Segatto, Suzanne Lancaster, Q. Duong, Francesco Driussi, L. Grenouillet, L. Triozon, Jean Coignus, Thomas Mikolajick, S. Slesazek, and D. Esseni, “Interplay between charge trapping and polarization switching in beol-compatible bilayer ferroelectric tunnel junctions,” *IEEE Journal of the Electron Devices Society* **10**, 1–1 (2022).
- [36] Riccardo Manenti, Eyob A. Sete, Angela Q. Chen, Shobhan Kulshreshtha, Jen-Hao Yeh, Feyza Oruc, Andrew Bestwick, Mark Field, Keith Jackson, and Stefano Poletto, “Full control of superconducting qubits with combined on-chip microwave and flux lines,” *Applied Physics Letters* **119**, 144001 (2021), <https://pubs.aip.org/aip/apl/article-pdf/doi/10.1063/5.0065517/13194475/144001.1.online.pdf>.
- [37] Alexander Bilmes, Serhii Volosheniuk, Alexey V. Ustinov, and Jürgen Lisenfeld, “Probing defect densities at the edges and inside josephson junctions of superconducting qubits,” *npj Quantum Information* **8** (2022), 10.1038/s41534-022-00532-4.
- [38] Jürgen Lisenfeld, Alexander Bilmes, Anthony Megrant, Rami Barends, Julian Kelly, Paul Klimov, Georg Weiss, John M. Martinis, and Alexey V. Ustinov, “Electric field spectroscopy of material defects in transmon qubits,” *npj Quantum Information* **5** (2019), 10.1038/s41534-019-0224-1.
- [39] J.-S Oh, C.J. Kopas, H. Canizoglu, E. Lachman, K. Yadvalli, J.Y. Mutus, T.-H. Kim, M.J. Kramer, A.H. King, and L.) Zhou, “Correlating aluminum layer deposition rates, josephson junction microstructure, and superconducting qubits’ performance,” (2024), in preparation.
- [40] Danièle Bouchet and Christian Colliex, “Experimental study of elnes at grain boundaries in alumina: intergranular radiation damage effects on al-l23 and o-k edges,” *Ultramicroscopy* **96**, 139–152 (2003).
- [41] S. Fritz, A. Seiler, L. Radtke, R. Schneider, M. Weides, G. Weiß, and D. Gerthsen, “Correlating the nanostructure of al-oxide with deposition conditions and dielectric contributions of two-level systems in perspective of superconducting quantum circuits,” *Scientific Reports* **8** (2018), 10.1038/s41598-018-26066-4.
- [42] S. Fritz, L. Radtke, R. Schneider, M. Luysberg, M. Weides, and D. Gerthsen, “Structural and nanochemical properties of alox layers in al/alox/al-layer systems for josephson junctions,” *Physical Review Materials* **3** (2019), 10.1103/physrevmaterials.3.114805.
- [43] K. Kimoto, Y. Matsui, T. Nabatame, T. Yasuda, T. Mizoguchi, I. Tanaka, and A. Toriumi, “Coordination and interface analysis of atomic-layer-deposition Al₂O₃ on Si(001) using energy-loss near-edge structures,” *Applied Physics Letters* **83**, 4306–4308 (2003), <https://pubs.aip.org/aip/apl/article-pdf/83/21/4306/12229282/4306.1.online.pdf>.
- [44] C Weigel, G Calas, L Cormier, L Galois, and G S Henderson, “High-resolution al l2, 3-edge x-ray absorption near edge structure spectra of al-containing crystals and glasses: coordination number and bonding information from edge components,” *Journal of Physics: Condensed Matter* **20**, 135219 (2008).

- [45] Mingqiang Li, Yidi Shen, Kun Luo, Qi An, Peng Gao, Penghao Xiao, and Yu Zou, “Harnessing dislocation motion using an electric field,” *Nature Materials* **22**, 958–963 (2023).
- [46] S. Alfonzetti, E. Diletto, and N. Salerno, “Simulated annealing with restarts for the optimization of electromagnetic devices,” *IEEE Transactions on Magnetics* **42**, 1115–1118 (2006).
- [47] Hideki Hashimoto, Yohei Onodera, Shuta Tahara, Shinji Kohara, Koji Yazawa, Hiroyo Segawa, Motohiko Murakami, and Koji Ohara, “Structure of alumina glass,” *Scientific Reports* **12**, 516 (2022).
- [48] Pablo G. Debenedetti and Frank H. Stillinger, “Supercooled liquids and the glass transition,” *Nature* **410**, 259–267 (2001).

Supplement for: Alternating Bias Assisted Annealing of Amorphous Oxide Tunnel Junctions

D. P. Pappas¹, M. Field¹, C. Kopas¹, J. A. Howard¹, X. Wang¹,
E. Lachman¹, Lin Zhou^{2,3}, Jinsu Oh^{2,3}, K. Yadavalli¹,
E. A. Sete¹, A. Bestwick¹, M.J. Kramer^{2,3}, J. Y. Mutus¹

¹*Rigetti Computing, 775 Heinz Avenue, Berkeley, CA 94710, USA*

²*Ames National Laboratory, Ames, IA 50011, USA*

³*Department of Materials Science and Engineering,
Iowa State University, Ames, IA 50011, USA*

February 28, 2024

1 Dependence of ABAA process on junction size

Typically two different-size junctions, connected in parallel, are used in order to make an asymmetric SQUID for qubit tunability. For these devices, it is important that the ABAA process works for both junctions in a similar manner. This hinges on the idea that the process is voltage-driven. To establish this, the ABAA process was conducted on similar, separate junctions. The data was taken for nominally identical parameters, i.e. voltage, pulse duration, and pulse number. Data from these studies is shown in Fig. 1(a) and (b). The statistical analysis, shown in Panel(b) demonstrates that the resistance increase, in percent, is weakly dependent on the size of this set of junctions. The mean values and uncertainties, 29 ± 1.9 for the large and 32 ± 3 for the small junctions, overlap. The Student T distributions indicate that the uncertainties are significant, hence it is important to take these differences into account when designing the SQUIDs.

2 Qubit spectroscopy and coherence

Strongly coupled TLS were studied using qubit spectroscopy of the tunable qubits across the flux period. While no strongly coupled TLS were observed in qubits treated by ABAA, in the unprocessed qubits, there were an average of 0.7 TLS/GHz seen in a 21-qubit ensemble with a 10 GHz total tunable range. Based on this, we would have expected to see $\sim 3 - 4$ TLS in the 9-qubit, 5.4 GHz tunable range of ABAA trimmed junctions. An example of a strongly-

coupled TLS in an untreated qubit is shown in Fig 2, with the avoided level fitting shown in Fig. 3.

In addition, we show a zoomed-in version of Fig.4(a) from the paper in Fig.4. While there are small features in the spectroscopy observed in this ABAA qubit, careful analysis shows that they are due to couplings with other qubits on the chip. The salient characteristic of these features is that there is no distinct splitting observed, as shown above, that would tie these to strongly coupled TLSs in the junction.

The frequency of one ABAA-treated qubit was measured over an extended time to evaluate the stability. The mean qubit frequency over the full duration of measurements, three days in total, is $4,280.56 \pm 0.001$ MHz. For the subset of the data shown in Fig. 5, two protocols were used. The first protocol, i.e. "slow" measurements, averaged the Ramsey oscillation frequency for 15-minute intervals, while the "fast" measurements used a much shorter, 15-second averaging interval. This was done to check if there were fast jumps that were not being resolved in the slow measurements. The standard deviation over the slow measurement dataset is 0.028 MHz, and it scaled as expected for the fast measurements. No fast jumps in the frequency were observed.

Tabulations of the ABAA-treated qubit coherence values, from the data (Fig.[5] from the main paper), are shown in Table 1.

Qubit Coherence	T_1 (μ s)	T_2^* (μ s)	T_ϕ (μ s)
ABAA treated	28.4 ± 8.7	34.1 ± 10.6	62.5 ± 23.1
80 °C annealed	20.9 ± 4.6	29.0 ± 12.7	37.9 ± 39.9
Unprocessed	19.5 ± 5.0	22.7 ± 12.3	41.4 ± 45.1

Table 1: Qubit coherence for ABAA treated, 80 ° C annealed and unprocessed qubits. The error bars are 1σ standard deviations.

3 Extracting junction critical currents

Critical currents were extracted using the transmon relations from Koch, et al.[koch2007charge]. Specifically, the anharmonicity, $\alpha = \omega_{01} - \omega_{12} \approx E_C$, and frequency, $\omega_{01} \approx \sqrt{8E_cE_J}$, relationships were used to find $I_0 = 2\pi E_J/\Phi_0$. The results of this are shown in Fig. 6

4 TEM characterization

Secondary electron images for the Josephson junction surface were acquired using a scanning electron microscope (SEM) (Helios, Thermo Fisher Scientific Ltd.) at 2 kV. Transmission electron microscope (TEM) samples were prepared by a focused ion beam instrument with a gas injection system (Helios, Thermo Fisher Scientific Ltd.). The TEM samples were thinned to electron

beam transparency by a Ga^+ ion beam from 30 to 2 kV. The TEM samples were investigated by an aberration-corrected TEM (Titan Cube, Thermo Fisher Scientific Ltd.) at 200 kV. A high-angle annular dark-field (HAADF) detector was used for dark-field imaging in scanning TEM (STEM) mode with a convergent semi-angle and a collection semi-angle of 18 mrad and 74-200 mrad, respectively. Energy-dispersive X-ray spectroscopy (EDS) and electron energy-loss spectroscopy (EELS) studies were carried out with probe currents of 250 nA and 50 nA, respectively. Dual EELS was performed to acquire all-electron energy-loss (ELL) spectra. The plural scattering effect of all the raw ELL spectra was removed via Fourier-ratio deconvolution.

The EELS data were taken from a typical thin spot of the barrier. We do not have EELS data from the areas around grain boundary regions, but from earlier work, we observe that the oxides are significantly thicker in those regions, and hence are not expected to participate in the tunneling process.

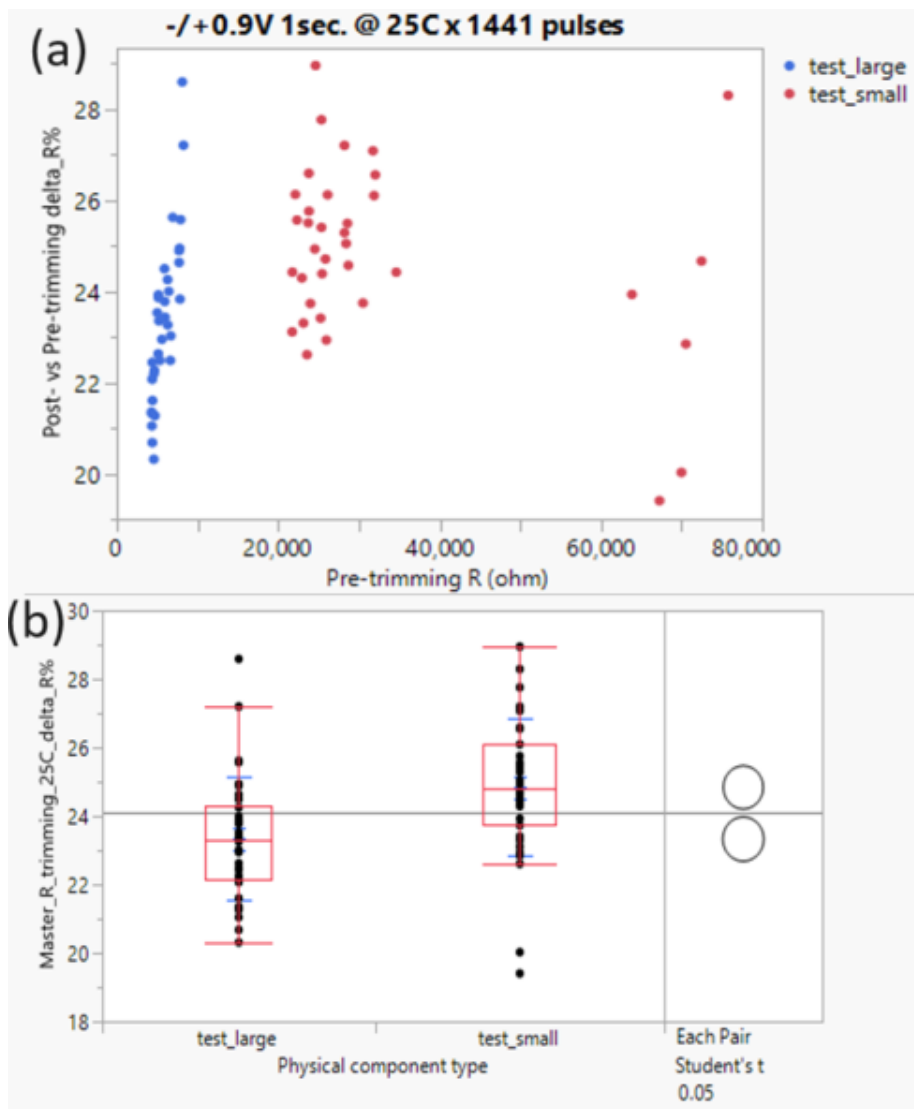


Figure 1: Dependence of ABAA trimming effect on junction resistance: Panel (a) Raw data showing resistance post-ABAA compared to resistance before. All data taken at 25 degrees; Panel (b) Date from panel (a) binned by the size of the junction with statistical analysis.

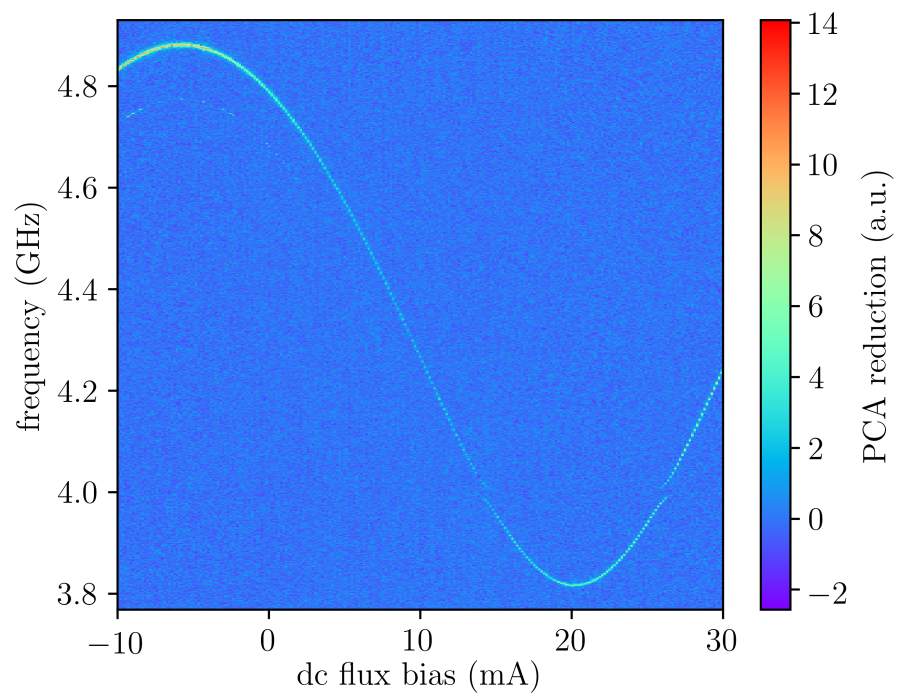


Figure 2: Untreated qubit spectroscopy illustrating a strongly coupled TLS near 4 GHz.

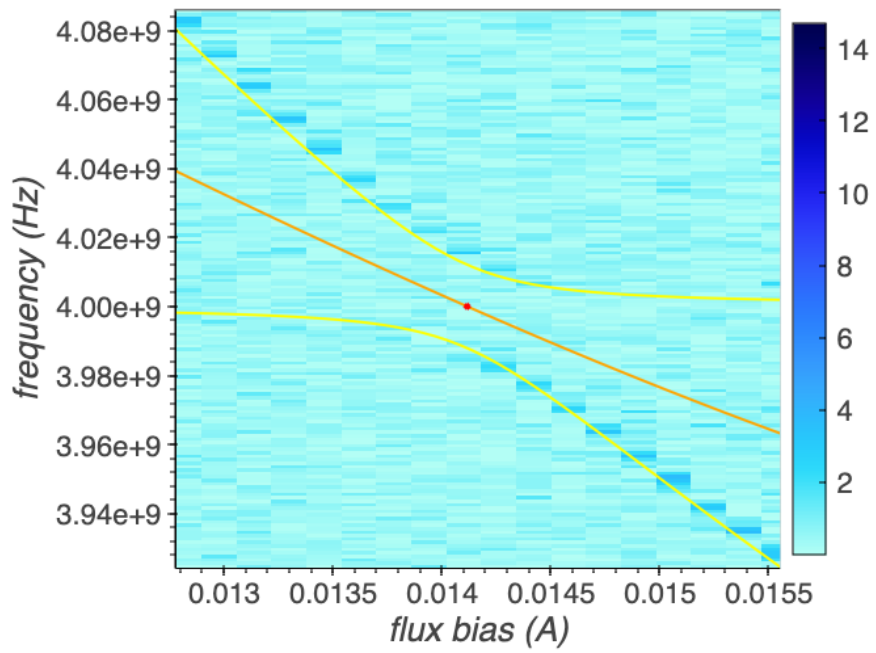


Figure 3: Fit to avoided level crossing for TLS in untreated qubit Fig. 2

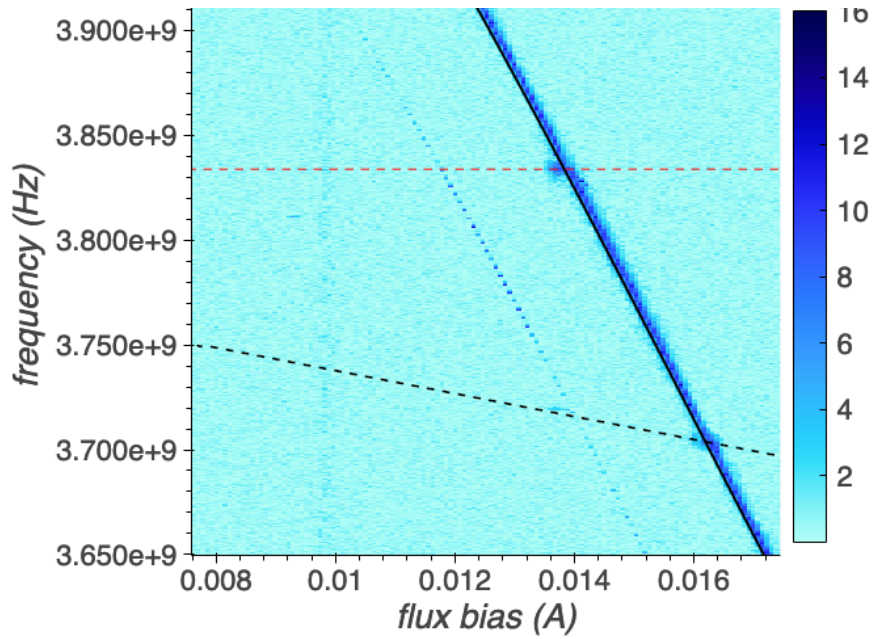


Figure 4: Zoomed in the region of data from an ABAA-tuned qubit showing faint features. The red dashed line is a nearest neighbor that is a fixed qubit, and the black dashed line is a nearby tunable qubit. The $f_{02}/2$ trace is visible 0.11 GHz below the f_{01} line

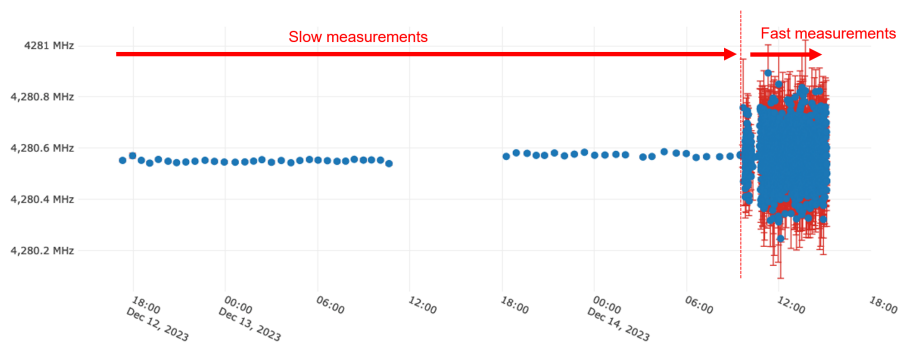


Figure 5: Time trace of a single frequency over an interval of about 46 hours.

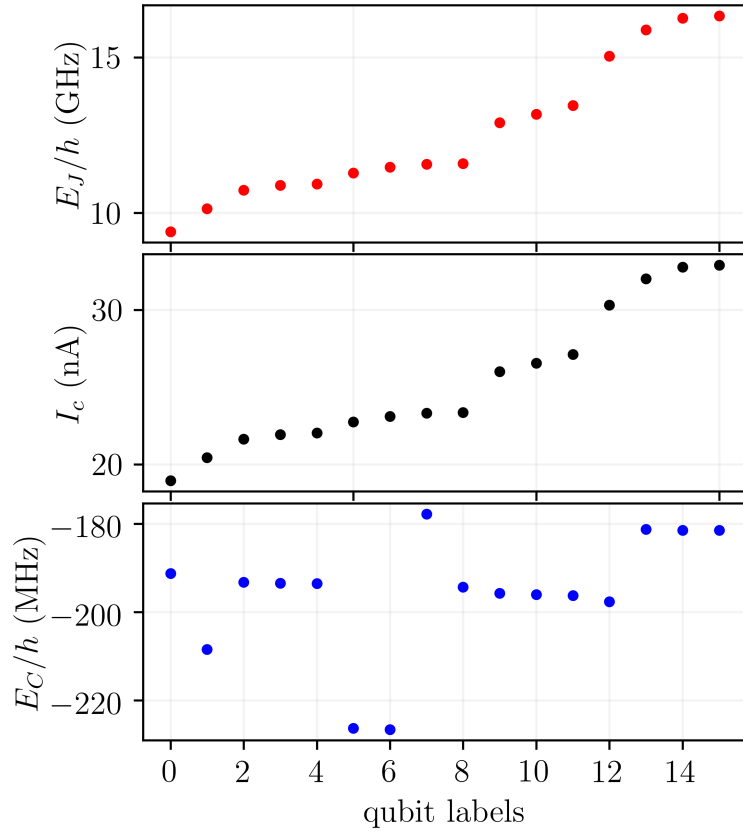


Figure 6: Top, center, and bottom panel show the values of E_J , I_0 , and E_C extracted from the data taken from the 15 ABAA-treated qubits.